Supplementary Information (SI) for Nanoscale.
This journal is © The Royal Society of Chemistry 2024

Electronic Supplementary Information

Boosting Quantum Efficiency and Suppressing Self-Absorption in CdS Quantum Dots through Interface Engineering

Shyamashis Das[a,d], Biswajit Bhattacharyya[a], Ashutosh Mohanty,[a] Poulomi Mukherjee[a], Arpita Mukherjee[a], Anirban Dutta[a], Anshu Pandey[a], Priya Mahadevan[b], Ranjani Viswanatha[c*] and D. D. Sarma[a*]*

[a] Solid State and Structural Chemistry Unit, Indian Institute of Science, Bengaluru 560012 (India).

[b] Department of Condensed Matter and Materials Physics , S.N. Bose National Centre for Basic Sciences, Block JD, Sector-III, Bidhannagar, Kolkata 700106 (India).

[c] New Chemistry Unit and International Centre for Materials Science and School of Advanced Materials, Jawaharlal Nehru Centre for Advanced Scientific Research, Jakkur, Bengaluru 560064 (India)

[d] Department of Chemistry, Ramananda College, Bankura University, Bishnupur 722122 (India)

***Corresponding Authors:**

sarma@iisc.ac.in

priya@bose.res.in

rv@jncasr.ac.in

Calculation of Quantum Yield

The absolute quantum yields of all CdS quantum dots were directly measured using an Edinburgh Instrument FLS920 Series Fluorescence Spectrometer, using an integrating sphere and a photomultiplier tube as the detector with a spectral coverage of 200-870 nm. The detection efficiency at each wavelength, determined using a calibrated light source, is a part of the Edinburgh FLS920 instrument software that evaluates the PLQY. The details of the procedure are given in the instrument manufacturer's Technical Note available at https://www.edinst.com/wp-content/uploads/2019/08/Technical-Note.pdf.

CdS QDs dispersed in octadecene, the solvent in which QDs were synthesized, were first centrifuged for 5 min and then a part of the supernatant was dissolved in n-hexane to attain an optical density of about 0.1 at the excitonic absorption. Typically, the solution of QDs dispersed in octadecene needed to be mixed with n-hexane at a volumetric ratio of 1:100 to achieve the desired optical density. For the instrument to calculate absolute quantum yields, first a spectrum of pure n-hexane was collected before recording the spectrum of QDs diluted in hexane. The blank data of hexane was used by the instrument as the reference to subtract the background. Then the PL spectrum of the diluted sample was collected to determine the absolute PL QY values reported here via the instrument software, discussed above.

Simulation of XRD Pattern

DIFFaX program[1] was used for simulation of XRD patterns of CdS QDs of various sizes with intergrowth planes. Intergrowth of WZ planes are introduced in the crystal along cubic [111] direction of ZB phase which is considered as crystallographic *c*-direction for simulation. Stacking vectors $\vec{R}_1$ (2/3, 1/3, 1/2) results in …ABCABC… type stacking producing ZB phase and $\vec{R}_2$ (1/3, 2/3, 1/2) results in ..*ABAB*.. type stacking producing WZ phase. To produce intergrowth plane, stacking vectors are alternated in such a way that ..*ABA*.. layers of WZ phase gets introduced into …ABCABC... stacking of ZB phase. Recursive mode of layer sequencing was used for simulations which allows calculations of diffraction intensities for a statistical ensemble of crystallites, each with a distinct stacking sequence, but weighted by a probability of occurrence for such a sequence. Stacking transition probability was varied as a parameter in the simulation. It has been found that the simulated diffraction pattern of intergrowth QDs with one layer of WZ phase (i.e. *ABA*

stacking) in an otherwise ..ABCABC.. stacking of ZB phase matches well with the experimental XRD pattern of intergrowth QDs. A finite length in the *ab*-plane of QDs is used to model its diameter. Along *c*-direction number of layers are restricted such a way that dimension along *c*-direction becomes almost equal to diameter in the *ab*-plane. Simulations were carried out for CdS QDs of sizes 3.3 nm, 4.0 nm and 4.7 nm to account for particle size distribution obtained from the size distribution analysis of TEM images (Figure S1). For each model with different extent of intergrowth planes, the final diffraction pattern is a weighted average of three sizes of the particles mentioned above. We have considered 25% weightage of the diffraction pattern of 3.3 nm particles, 50% weightage of 4 nm particles and 25% weightage of 4.7 nm particles to calculate simulated diffraction pattern in each case.

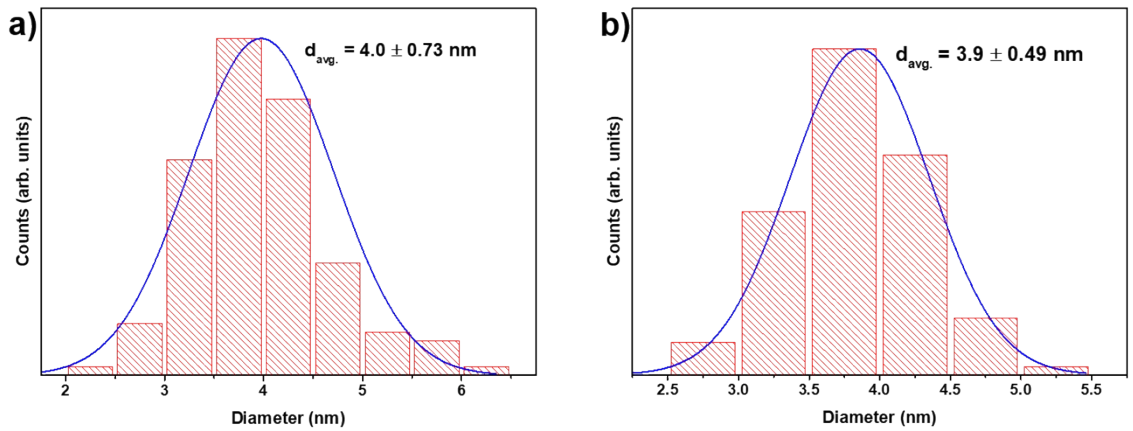

Figure S1. Particle size distribution histograms of the TEM images shown in Figures 1(a) and 1(b) are shown in (c) and (d), respectively.

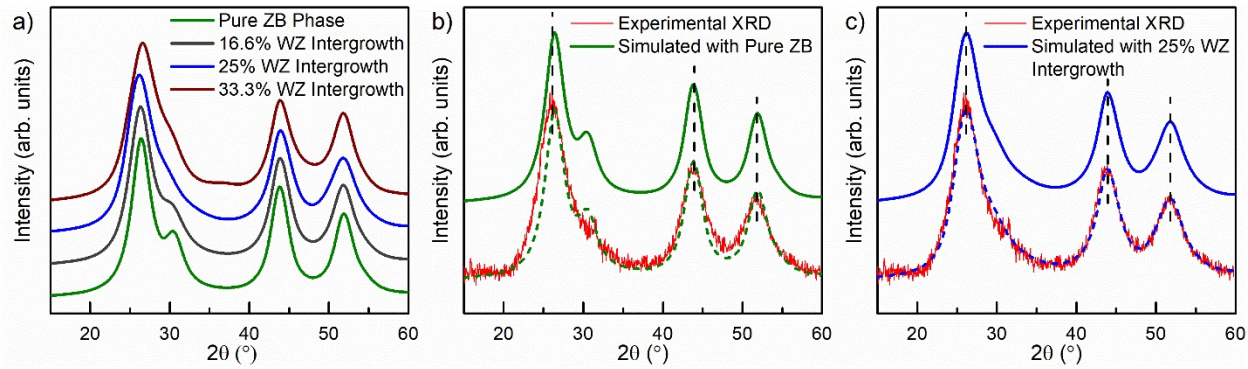

Figure S2. (a). Simulated XRD patterns of ~4 nm zinc blende CdS QDs with different extents of wurtzite intergrowth planes. The simulation accounts for the size distribution observed in the TEM (see Figure S1(b)) as described in the text. A comparison of experimental XRD pattern (red line) of CdS QDs containing intergrowth planes with simulated pattern (b). of pristine CdS QDs in pure zinc blende phase (green line) and (c). of 25% wurtzite intergrowth layers (blue line). The dashed lines in (b) and (c) are vertically adjusted simulated XRD patterns to overlap the experimental data (red line) of the CdS QD containing intergrowth planes. The vertical dashed lines are guide to help in comparing the peak positions.

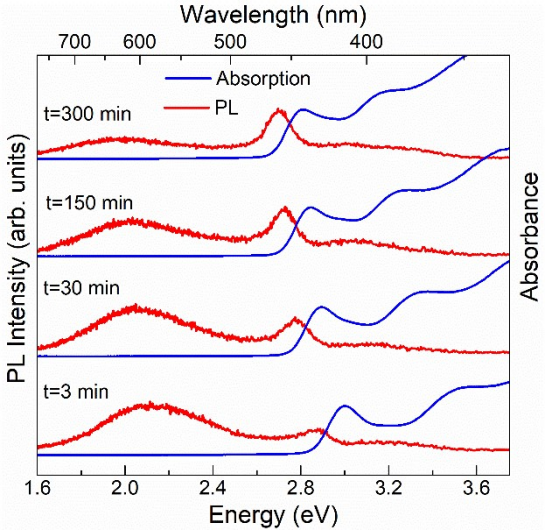

Figure S3. Optical absorption and PL spectra of CdS quantum dots annealed at 250 °C for varying intervals of time, showing a systematic decrease in the intensity of the lower energy, interface emission and a concomitant increase in the intensity of the higher energy excitonic emission on annealing. The systematic shift of the absorption peak to lower energies with the increasing annealing time reflects the growth of the QDs on prolonged annealing via Ostwald ripening.

Synthesis and Characterization of Core-shell QDs:

ZnS shell on CdS QD cores was achieved by thermal-cycling coupled single-precursor (TC-SP) method reported earlier[2] using zinc diethyldithiocarbamate ($Zn(DDTC)_2$) as the single precursor. The precursor solution was prepared by dissolving 0.362 g (1 mmol) of $Zn(DDTC)_2$ in 10 ml oleylamine. For preparation of CdS/ZnS core-shell QDs, first freshly synthesized interface-engineered CdS QDs were thoroughly washed with ethanol to remove any unreacted Cd- and S-precursors. TEM analysis (Figures 1b and S1b) shows the diameter of these CdS QDs to be ~3.9 nm. $\sim 10^{-7}$ mol of these CdS QDs were re-dispersed in 10 ml 1-octadecene (1-ODE), degassed thoroughly in vacuum and heated to 50 °C in Ar atmosphere. 0.44 ml $Zn(DDTC)_2$ solution was added at this stage and temperature was increased to 180 °C. The reaction mixture was heated in Ar atmosphere at 180 °C for 20 min to allow the growth of ZnS monolayer. After the synthesis, the resulting QDs were cooled to room temperature. These core-shell QDs were cleaned with ethanol to remove all organic reactants used for the synthesis and re-dispersed in n-hexane to record optical absorption and emission spectra, and TEM images. Figure S4a shows TEM images of CdS/ZnS core-shell QDs. A comparison of size distribution analyses of core-only CdS QDs (Figure S1b) and that of CdS/ZnS core-shell QDs (Figure S4b) confirm an increase in the average particle size following the growth of the ZnS shell.

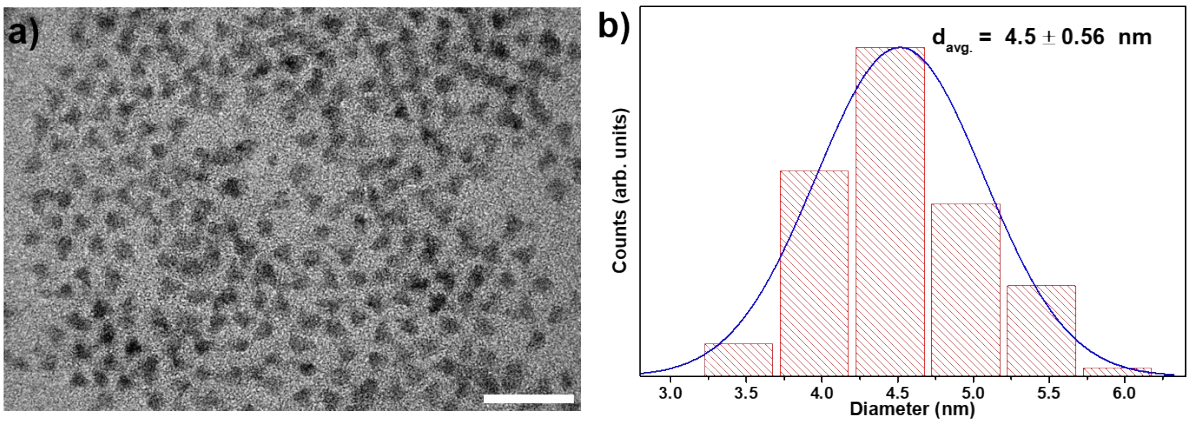

Figure S4. (a) TEM images of CdS QDs after overcoating with ZnS. (b) Corresponding particle size distribution histograms for core-shell QDs. Scale bar in image (a) is 20 nm.

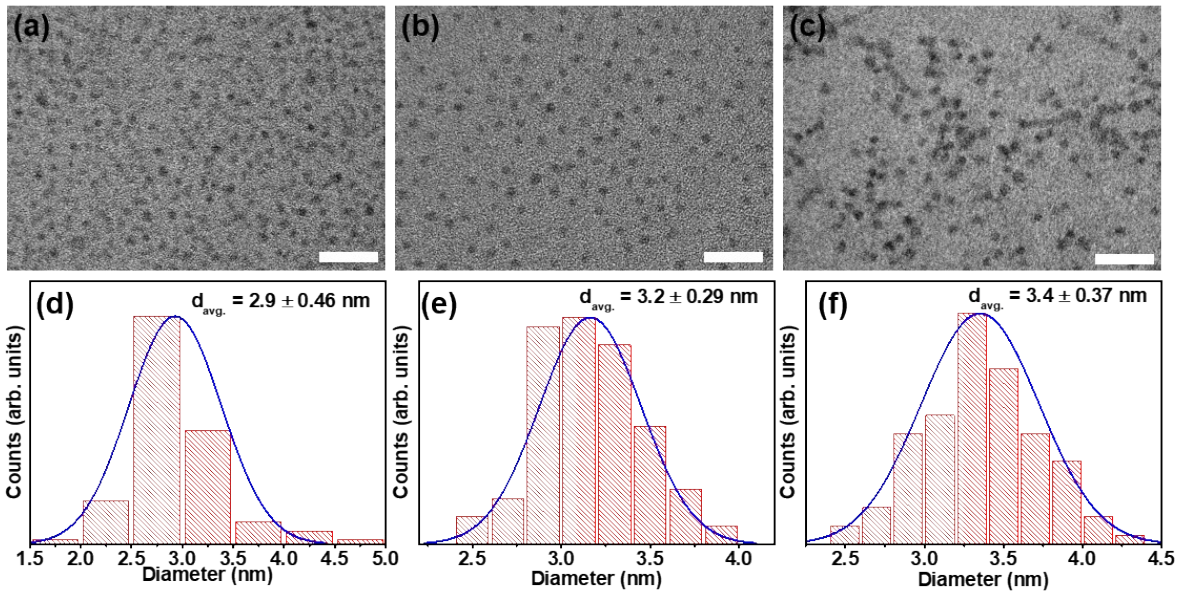

Figure S5. (a) – (c) TEM images of CdS nanocrystals with intergrowth planes of three different sizes. (d) – (f) Corresponding particle size distribution histograms. Average diameter of particles of each sample is extracted by fitting distribution of histograms with gaussian function. Scale bars in the TEM images (a) – (c) are 20 nm in length in each case.

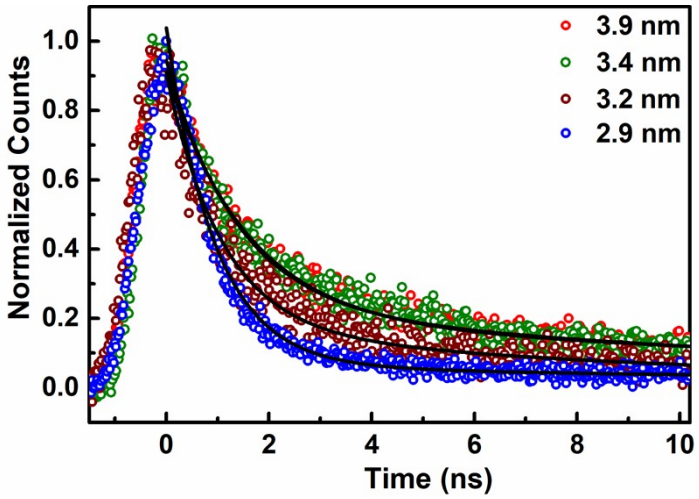

Figure S6. Photoluminescence decays of band-edge emission of interface-engineered CdS QDs of four different sizes. Each of the decay profiles was fit with a bi-exponential function $A_1^{'}exp\left(-t/\tau_1^{'}\right) + A_2^{'}exp\left(-t/\tau_2^{'}\right)$. The black lines represent bi-exponential fit to each decay profile.

Table S1. Results of biexponential fitting of photoluminescence decay of band-edge emission of four different sizes of interface-engineered CdS QDs.

Diameter (nm)	$E_{Emission}$ (eV)	$A_1^{'}\tau_1^{'}$ (%)	$\tau_1^{'}$ (ns)	$A_2^{'}\tau_2^{'}$ (%)	$\tau_2^{'}$ (ns)
2.9	3.16	43.9	0.94	56.1	18.3
3.2	3.01	30.5	1.1	69.5	10.6
3.4	2.87	21.8	1.4	78.2	15.3
3.9	2.81	22.2	1.5	77.8	19.2

Table S2. Results of fitting of upconversion photoluminescence data.

Nature of Emission	Band-edge Emission		Intergrowth State Emission	
Function	$f(t) = A_1 e^{-t/\tau_1} + A_2 e^{-t/\tau_2}$		$f(t) = A_1 + A_2\left(1 - e^{-t/\tau_3}\right)$	
Fitting Parameters	A_1	0.4	A_1	0.01
	$\tau_1\,(fs)$	780 ± 33	A_2	0.4
	A_2	0.6	$\tau_3(fs)$	780 ± 10
	$\tau_2\,(fs)$	> 3000		

Joint density of state and calculation of band gap

Optical absorption spectra correspond to transitions from occupied to unoccupied states. This can be generated by summing up the individual dipole allowed transitions ($S_{l\to l\pm1}(\varepsilon)$) that is known to dominate the optical absorption spectra in the following way[3]

$$S_{l\to l\pm1}(\varepsilon) \propto \int_{E_F-\varepsilon}^{E_F} \rho_l(\varepsilon')\rho_{l\pm1}(\varepsilon'+\varepsilon)d\varepsilon'$$

where ρ_l and $\rho_{l\pm1}$ are partial density of states (PDOS) corresponding to angular momentum components l and $l\pm1$, respectively. The specific limits of integration make sure ρ_l are PDOS of occupied states and $\rho_{l\pm1}$ are PDOS of unoccupied states; hence, $S_{l\to l\pm1}$ represents joint density of states between occupied and unoccupied states. This quantity is proportional to the absorption probability and hence, when calculated over a span of energy represents simulated absorption spectra with the assumption of a constant dipole matrix element over the energy window considered. Representative plots of such joint densities of states are shown in Figures S7a and S7b for 4.2 nm sized pristine and interface engineered CdS quantum dots, respectively.

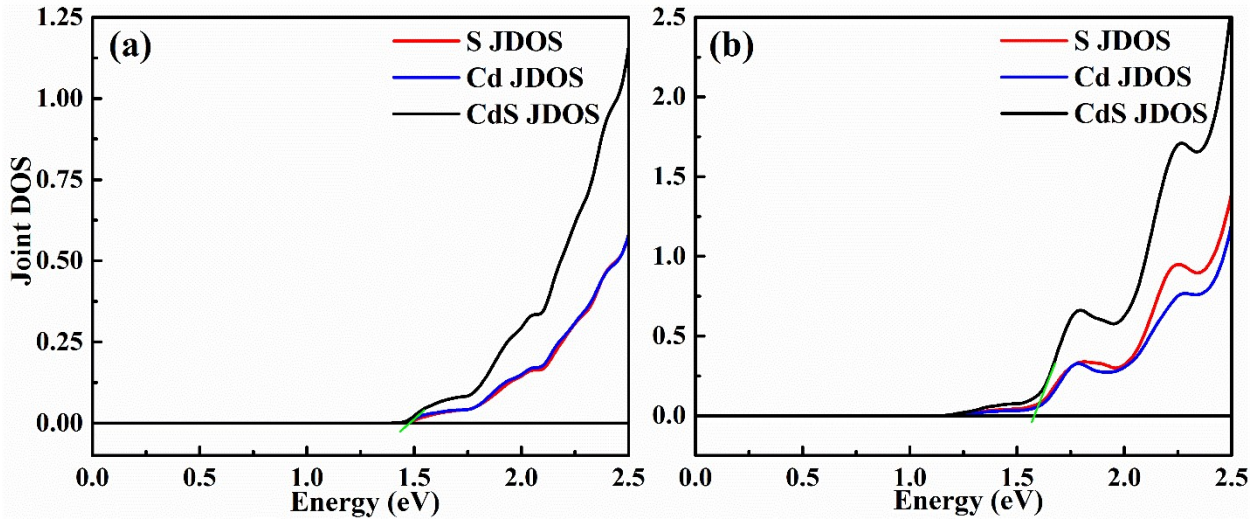

Figure S7. Calculated joint density of states of (a) pristine QD and (b) QD with intergrowth planes of ZB and WZ. The intersection of horizontal line parallel to energy axis and the green tangent line to the total JDOS indicate position of band gap of respective QD.

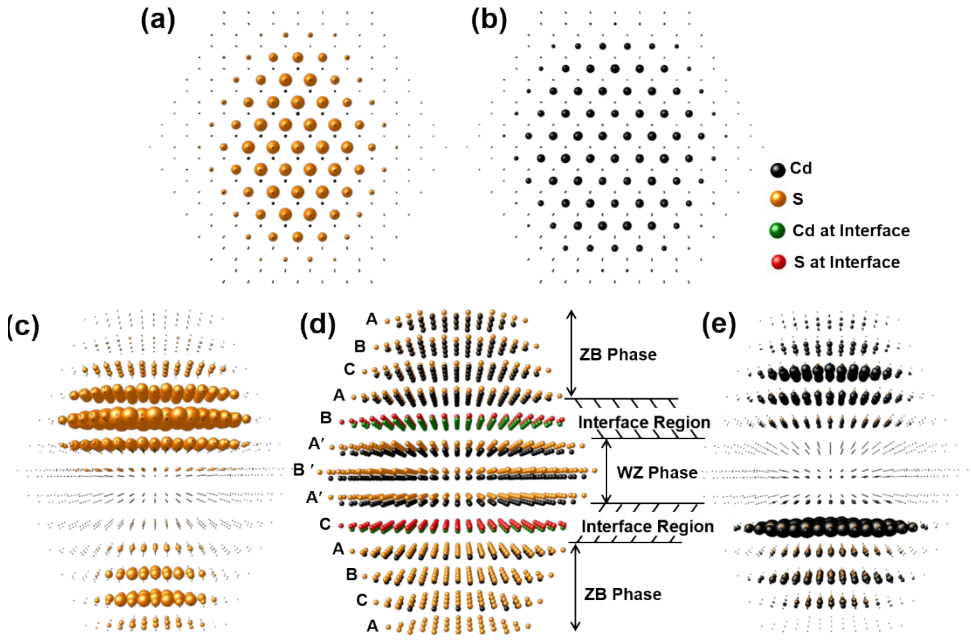

Figure S8. A view from perpendicular direction of [111] crystallographic axis of weights of the wave-functions for (a) the top of the occupied states (TOS) and (b) the bottom of the unoccupied states (BUS) of the CdS quantum dots (QDs) present in pure zinc blende (ZB) phase. Corresponding wave-function weights for (c) TOS and (e) BUS of CdS QDs of similar size as for ZB CdS QDs with results in panels (a) and (b) but with an intergrowth phase. A 3D plot of atomic co-ordinates of the CdS QD with intergrowth phases is shown in (d) with labels of ZB planes, wurtzite (WZ) planes and interface region.

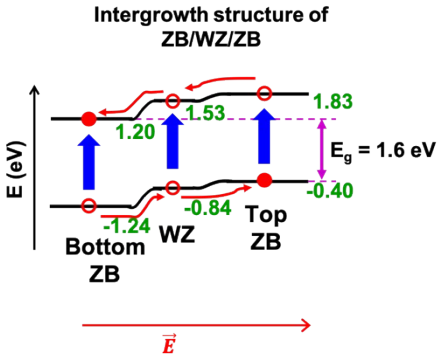

Figure S9. Energy level alignment of band edges of nanoclusters with ZB(6)-WZ(3)-ZB(6) intergrowth arrangement, obtained from ab-initio calculations using hybrid HSE06 functionals. Numbers in the parenthesis represent number of layers in ZB and WZ phases in the intergrowth nanocluster. Calculated energies of each individual level are marked in green in the figure.

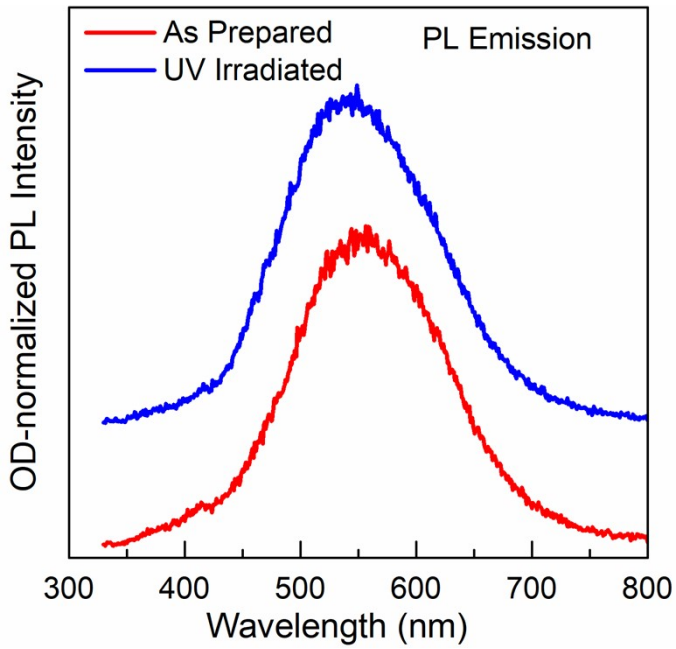

Figure S10. OD normalized photoluminescence spectra of interface engineered CdS QDs before and after irradiation of the sample with a 4 W UV lamp (λ_{UV} =405 nm) for 6 hours. The post-radiated spectrum is rigidly shifted vertically for clarity.

References

[1] M. M. J. Treacy, J. M. Newsam and M. W. Deem, *Proc. R. Soc. Lond. A* 1991, **433**, 499-520.

[2] D. Chen, F. Zhao, H. Qi, M. Rutherford and X. Peng, *Chem. Mater.*, 2010, **22**, 1437-1444.

[3] S. Gokhale, S. R. Barman and D. D. Sarma, *Phys. Rev. B* 1995, **52**, 14526-14530.